Title

Mitochondrial Dysfunction, Oxidative Stress, and Apoptosis Revealed by Proteomic and Transcriptomic Analyses of the Striata in Two Mouse Models of Parkinson's Disease

Journal

Journal of Proteome Research, 7(2)

ISSN

1535-3893

Authors

Chin, Mark H

Qian, Wei-Jun

Wang, Haixing

et al.

Publication Date

2008-02-01

DOI

10.1021/pr070546l

Published in final edited form as:
J Proteome Res. 2008 February ; 7(2): 666–677. doi:10.1021/pr070546l.

Mitochondrial Dysfunction, Oxidative Stress, and Apoptosis Revealed by Proteomic and Transcriptomic Analyses of the Striata in Two Mouse Models of Parkinson's Disease

Mark H. Chin[†,‡], **Wei-Jun Qian**[§], **Haixing Wang**[§], **Vladislav A. Petyuk**[§], **Joshua S. Bloom**[†], **Daniel M. Sforza**[|], **Goran Laćan**[†], **Dahai Liu**[⊥], **Arshad H. Khan**[†], **Rita M. Cantor**[‡], **Diana J. Bigelow**[§], **William P. Melega**[†], **David G. Camp II**[§], **Richard D. Smith**[§], and **Desmond J. Smith**[*,†]

[†]Department of Molecular and Medical Pharmacology, David Geffen School of Medicine at University of California—Los Angeles (UCLA), Los Angeles, California 90095

[‡]Department of Human Genetics, Laboratory of NeuroImaging, David Geffen School of Medicine at University of California—Los Angeles (UCLA), Los Angeles, California 90095

[§]Biological Sciences Division and Environmental Molecular Sciences Laboratory, Pacific Northwest National Laboratory (PNNL), Richland, Washington 99352

[|]Department of Neurology, David Geffen School of Medicine at University of California—Los Angeles (UCLA), Los Angeles, California 90095

[⊥]Department of Surgery, David Geffen School of Medicine at University of California—Los Angeles (UCLA), Los Angeles, California 90095

Abstract

The molecular mechanisms underlying the changes in the nigrostriatal pathway in Parkinson's disease (PD) are not completely understood. Here, we use mass spectrometry and microarrays to study the proteomic and transcriptomic changes in the striatum of two mouse models of PD, induced by the distinct neurotoxins 1-methyl-4-phenyl-1,2,3,6-tetrahydropyridine (MPTP) and methamphetamine (METH). Proteomic analyses resulted in the identification and relative quantification of 912 proteins with two or more unique peptides and 86 proteins with significant abundance changes following neurotoxin treatment. Similarly, microarray analyses revealed 181 genes with significant changes in mRNA, following neurotoxin treatment. The combined protein and gene list provides a clearer picture of the potential mechanisms underlying neurodegeneration observed in PD. Functional analysis of this combined list revealed a number of significant categories, including mitochondrial dysfunction, oxidative stress response, and apoptosis. These results constitute one of the largest descriptive data sets integrating protein and transcript changes for these neurotoxin models with many similar end point phenotypes but distinct mechanisms.

[*]To whom correspondence should be addressed. dsmith@mednet.ucla.edu.

Supporting Information Available: Significantly decreased DA levels in the striata of treated versus untreated animals (Supplementary Figure 1), gene set enrichment analysis for three significant categories from the LC–FTICR–MS data: ATP metabolism, protein degradation, and cell movement (Supplementary Figure 2), codon usage analysis for efficiently and inefficiently translated genes (Supplementary Figure 3), all quantified proteins (Supplementary Table 1), annotated list of significantly changed proteins in response to neurotoxin (Supplementary Table 2), significantly up- and downregulated transcripts in both MPTP- and METH-treated mice (Supplementary Table 3), efficiently translated genes (Supplementary Table 4), and miRNAs whose targeted genes had significantly different expression levels between treated and untreated striata (Supplementary Table 5). This material is available free of charge via the Internet at http://pubs.acs.org.

Keywords

Parkinson's disease; transcriptomics; proteomics; codon usage; miRNA; mouse model

Introduction

Parkinson's disease (PD) is a progressive, neurodegenerative disorder primarily affecting the extrapyramidal motor system of the central nervous system (CNS). The disorder is marked by the loss of nigrostriatal dopamine (DA) neurons in the substantia nigra pars compacta (SN), resulting in a significant decrease of DA content in the striatum. The diminished DA content is thought to be responsible for the effects of the disease on movement, including akinesia, rigidity, and tremors.[1,2] Increased DA production using 3,4-dihydroxy-L-phenylalanine (L-DOPA) is the standard treatment for PD patients but has adverse long-term effects. Despite intensive research, the exact cause of PD and the mechanisms that lead to nigrostriatal dopaminergic neuron death remain largely elusive; however, evidence suggests the potential role of mitochondrial dysfunction and oxidative stress in the pathogenesis of PD.[3,4] Thus, a deeper understanding of disease pathology at the molecular level is urgently needed.

Technological advances have allowed new assessments of disease pathology at a genomic scale, particularly in mouse models of brain disease. These developments have provided new insights into the associated molecular pathways of neurodegeneration.[5-9] Large-scale analysis is also possible for proteins in brain disorders using mass-spectrometry (MS)-based proteomics.[10] Proteomic profiling using 2D gel electrophoresis coupled with MS has been applied to Parkin-deficient mice and revealed several proteins involved in mitochondrial dysfunction and oxidative stress.[11] However, there have been few studies that compare in parallel the transcriptomic and proteomic changes in neurodegeneration.

Here, we investigate the striatal protein abundance and gene expression changes for two different toxicological mouse models of PD created using 1-methyl-4-phenyl-1,2,3,6-tetrahydropyridine (MPTP) and methamphetamine (METH). MPTP has been shown to induce Parkinsonism in mice with recapitulation of the hallmark cellular pathology, death of dopaminergic neurons in the SN, which decreases DA input to the target organ, the striatum.[12,13] MPTP probably acts through the inhibition of oxidative phosphorylation in dopaminergic neurons. [14] METH-treated mice also exhibit cell death of dopaminergic neurons in the SN, and although the parallels to the human disease are less strong, the behavioral traits in the mice are akin to PD patients.[15,16] METH stimulates catecholamine release, although the mechanisms by which large doses result in a PD model are unclear.[17,18]

We evaluated protein and transcript abundance changes in the striatum of the two mouse models using liquid chromatography (LC)–MS and microarrays, respectively. To date, this is the most comprehensive, integrated data set examining these two models of PD. The data provide insights into the physiological consequences of neurotoxicity and the potential molecular changes in the striatum of PD patients. In particular, we observed downregulation of a number of proteins and genes involved in mitochondrial dysfunction and oxidative response in the striatum. Furthermore, downregulation of several antiapoptotic and upregulation of pro-apoptotic proteins/genes was observed, also implicating programmed cell death in the disorder.

Experimental Procedures

Drug Models of PD

Adult C57BL/6J male mice (8 week, 21–27 g) received four i.p. injections of MPTP-HCl (15 mg/kg per injection), METH-HCl (10 mg/kg per injection), or 200 μL of 0.9% sterile saline (Con) at 2 h intervals.[18-20] Striata were bilaterally removed 7 days following injections, and samples were frozen immediately in liquid nitrogen.

Neurochemistry

Neurochemical parameters were obtained from a small portion of the left striatum of each mouse used for microarray analyses. Striatum samples were weighed wet, sonicated with 250 μL of 0.1 M perchloric acid, and centrifuged at 14 000 rpm for 15 min (4 °C). The supernatant was filtered through a 0.2 μm polytetrafluoroethylene (PTFE) filter, and an aliquot was diluted with water (1:2) for high-performance liquid chromatography (HPLC) analysis. The solid pellet was suspended in 1.0 mL of 0.2 M NaOH for the protein assay. For HPLC, we used an ESA Biosciences HPLC model 580 solvent delivery module (dual-piston pump) and an ESA Biosciences Coulochem II electrochemical detector with an analytical cell operating at +350 mV and 500 nA. The mobile phase consisted of acetonitrile/sodium phosphate monobasic buffer [75 mM sodium phosphate, 1.8 mM 1-octanesulfonic acid sodium salt (OSA), and 12 μM ethylenediaminetetraacetic acid, disodium salt dehydrate (EDTA)] at 9.5:90.5 (v/v) and pH 3.1 (aqueous phase). The guard column was Adsorbosphere HS, C18, 7.5 × 4.6 mm, 3 μm. Both columns were from Alltech Associates, Inc. The flow rate was 0.8 mL/min, and the injector loop volume was 20 μL.

Proteomic Analysis

For each mouse, the isolated striatal samples from the left and right brain were pooled, which provides an average ~20 μg of wet tissue. All striatal samples were homogenized and digested into peptides as previously described.[10] Peptides from control mice were individually labeled with ^{16}O, and peptide samples from MPTP- or METH-treated mice were individually labeled with ^{18}O using postdigestion immobilization trypsin-catalyzed labeling as previously described ($n \geq 5$, each group).[21] After labeling, an aliquot of the control sample (~150 μg/aliquot) was mixed with an equal amount of either an ^{18}O-labeled MPTP- or METH-treated sample. A total of 10 pairs of $^{16}O/^{18}O$-labeled peptide samples were thus generated with 5 replicates for each neurotoxin. The labeled peptide samples were further subjected to cysteinyl-peptide enrichment (CPE) as described previously[22] to generate a cysteinyl (Cys) fraction and a noncysteinyl (non-Cys) fraction for each sample. Both the Cys and non-Cys peptide samples were analyzed using a custom-built capillary LC system coupled online using an in-house manufactured electrospray ionization (ESI) interface to an 11.5 T Fourier transform ion cyclotron resonance (FTICR) mass spectrometer.

The analyses of quantitative LC–FTICR data sets were as previously described.[21] The detected LC–MS features were identified as peptides by matching the normalized elution time (NET) and accurate mass measurements to the pre-established accurate mass and time (AMT) tag database within a 5 ppm mass error and a 2% NET error and were quantified on the basis of $^{16}O/^{18}O$ intensity ratios. The AMT tag database was created by global 2D LC–MS/MS profiling of the whole mouse brain as previously described.[21] All abundance ratios were $\log_2$-transformed, and a global normalization between data sets was applied by shifting the mean log ratio of each data set to zero. The peptide identification and quantification results from Cys and non-Cys data sets were combined to achieve increased proteome coverage as well as protein sequence coverage. All quantified peptides were rolled up to nonredundant protein groups using ProteinProphet,[23] and the abundance ratio for each

protein group was calculated by averaging the ratio of multiple unique peptides stemming from the same protein group.[24]

A one-sample *t* test was applied for both protein abundance ratios and peptide abundance ratios against a mean value of zero to determine whether the protein displayed significant abundance changes following each neurotoxin treatment. A two-sample *t* test was applied to detect abundance differences between the two models. A protein is considered to have a significant abundance change when the protein has a *p* value less than 0.05 with at least two different peptides, with both showing a relatively good peptide level *p* value (average *p* value < 0.2).

Microarray Analysis

Gene expression data were obtained from the pooled left and right striata of the three groups of mice: MPTP, METH, and Con ($n = 3$, each group). Gene expression levels were obtained using GeneChip Mouse Genome 430A 2.0 array (Affymetrix, Inc., Santa Clara, CA). Striatum cDNA samples were prepared using the One-Cycle cDNA synthesis kit (Affymetrix, Inc.) according to the protocol of the manufacturer, with RNA from one mouse being applied to one microarray. Our complete data set is deposited in the Gene Expression Omnibus database (accession number GSE8030; http://www.ncbi.nlm.nih.gov/geo/).

A one-sample *t* test was applied for transcript abundance ratios against a mean value of zero to determine whether the transcript was significantly different, following each neurotoxin treatment. A two-sample *t* test was applied to detect transcript abundance differences between the two models. A false discovery rate (FDR) was used to adjust for multiple hypothesis testing in R (http://faculty.washington.edu/jstorey/qvalue/).[25,26]

Gene Set Enrichment Analysis

To detect groups of proteins having statistically significant concordant changes, we used gene set enrichment analysis (GSEA).[27] The data set was first screened against Gene Ontology (GO), Kyoto encyclopedia of genes and genomes (KEGG), and other annotations using http://www.babelomics.org.[28] For proper handling of the missing values and estimation of the confidence of the changes for the selected groups, we performed a sign test using the BSDA package of the R environment for statistical computing (www.r-project.org).[29]

Results

Dopamine Depletion in Neurotoxin-Treated Striata

C57/BL6J mice were treated with MPTP, METH, or saline (control) ($n = 5$, each group, MS; $n = 3$, each group, microarrays). A small portion of the left striatum from each mouse was sampled using HPLC. A significant loss of DA and its metabolites was observed in MPTP- (55% decrease, *t* test $= 1.81 \times 10^{-4}$, df $= 1$, $p < 0.0002$) and METH-treated animals (71% decrease, *t* test $= 2.21 \times 10^{-4}$, df $= 1$, $p < 0.0003$), while levels of a different neurotransmitter, serotonin, and its metabolites remained unchanged (Supplementary Figure 1 in the Supporting Information).

Proteomic Abundance Profiling

To analyze the potential neurotoxin-induced protein abundance changes, we applied a global quantitative proteomic approach (Figure 1), which integrates $^{16}O/^{18}O$ labeling and Cys-peptide fractionation with the AMT tag strategy to achieve relatively good proteome coverage with quantification.[21] Striata from MPTP, METH, and control mice were individually processed and labeled, which led to the generation of 10 $^{16}O/^{18}O$-paired

samples. Each sample was fractionated into Cys and non-Cys samples, which were individually analyzed by LC–MS to identify statistically significant changes. An extensive mouse brain peptide/protein database was recently developed from a global characterization of the mouse brain proteome by liquid chromatography coupled with tandem mass spectrometry (LC–MS/MS).[10]

The analyses resulted in the identification of ~4600 unique peptides corresponding to 1614 proteins, with all proteins quantified in at least 4 of the 10 paired biological samples. Relative protein abundance is expressed as a ratio of neurotoxin-treated to control sample levels. Figure 2A shows the overall reproducibility of the analyses by comparing the correlation of the raw peptide intensities (only ^{18}O intensities were used) between any two biological samples. As shown, the Pearson correlation coefficient is 0.94 ◦ 0.02 within the same METH or MPTP models (intratoxin), while the observed correlation coefficient 0.89 ◦ 0.03 between the two models (intertoxin) is slightly lower, as expected. The results suggest overall good reproducibility of the quantitative data.

Statistical analyses confidently identified 912 proteins with at least two unique peptides among the total 1614 proteins. Using a Student's *t* test, 199 and 149 proteins were identified with expression ratios significantly different from a $\log_2$ ratio of zero (p values < 0.05) in MPTP and METH models, respectively. To reduce false positives, this list of proteins was further filtered by requiring the $\log_2$ ratio to be at least 0.3 (25% change) and good agreement between multiple peptides detected from the same peptides (average peptide p value < 0.2). A final list of 86 proteins had significant abundance changes following neurotoxin treatment. The lists of the total 1614 proteins and the 86 proteins with significant abundance changes are supplied as Supplementary Table 1 and Table 1/Supplementary Table 2 (Supplementary Tables are in the Supporting Information), respectively.

Figure 2B shows a heatmap of the abundance patterns for the proteins with significant changes. A large percentage of proteins displayed consistent abundance regulation in both the MPTP and METH-treated mice. The consistency between samples extended to multiple peptides detected from the same protein (Figure 2C). Parts A and B of Figure 3 show examples of significantly up- and downregulated proteins in MPTP- and METH-treated striata, respectively. Consistent with this observation, a significant correlation (R ➲ 0.6563, p < 10^{-20}) was found in protein abundance changes in response to both neurotoxins (Figure 3C). One example illustrating the sensitivity of detection of quantitative protein changes is Purkinje cell protein 4 (Pcp4), for which we detected an average $\log_2$ downregulation of −0.44 ◦ 0.18 (p ➲ 0.004) in MPTP (a 28% decrease) and −0.25 ◦ 0.13 (p ➲ 0.035) in METH. This agrees well with a recent report of a ~30% decrease following MPTP.[30]

Gene Expression Profiling

Transcript profiling of the striatum was performed for each of the three conditions using Affymetrix 430A 2.0 microarrays, with the pooled left and right striatum of one animal analyzed using one array. Following robust multichip analysis (RMA) normalization of the data across all experiments, we identified 34 significant differentially expressed genes (FDR < 0.05) that were upregulated and 29 downregulated genes in the MPTP experiment compared to control samples. We also identified 51 and 40 genes up- and downregulated in the METH-treated striata, respectively (FDR < 0.05). The two gene lists with transcript abundance changes are in Supplementary Table 3 in the Supporting Information. A significant overlap was also found between the striatal responses to MPTP and METH, with 17 upregulated and 10 downregulated genes shared between the two treatment groups (x^2 ➲ 10^4, df ➲ 1, p < 0.001). These genes likely represent a common response of the striatum to the loss of dopaminergic afferents caused by the two different neurotoxins (parts A and B of Figure 4).

Consistent with the overlap among the significant genes between MPTP and METH, significant correlation (R ➲ 0.718, $p < 10^{-16}$) was also found between all gene expression changes for both neurotoxin treatment conditions (Figure 4C). Such consistency between MPTP and METH agrees well with the proteomic observation, which is anticipated from the similar biological consequences of the two neurotoxin treatments. One of the genes upregulated in common between MPTP and METH was glial fibrillary acidic protein (Gfap), where similar abundance changes at the protein level were also observed. Gfap is an astrocyte marker known to be upregulated in acute traumatic brain injury and neurological diseases.[31,32]

We used qRT-PCR analyses of MPTP- and METH-treated striata to confirm the expression changes for two of the most significant differentially regulated genes common to the two toxins, Gfap and related RAS viral (r-ras) oncogene homologue 2 (Rras2) (Figure 4D). Similar to the microarray results, Gfap and Rras2 were significantly upregulated compared to controls in response to both MPTP and METH treatments as judged using qRT-PCR (Gfap, t ➲ 0.489, df ➲ 1, p ➲ 0.035, MPTP and t ➲ 0.487, df ➲ 1, p ➲ 0.048, METH; Rras2, t ➲ 0.491, df ➲ 1, p ➲ 0.029, MPTP and t ➲ 0.489, df ➲ 1, p ➲ 0.036, METH).

Comparison of Protein and Transcript Data

When the genes showing significant transcript and protein abundance changes were compared, only two, Gfap and glutathione peroxidase 4 (Gpx4), displayed significant abundance changes at both the transcript and protein level. Gpx4, an antioxidant defense enzyme previously reported to have a protection role in oxidative stress-induced apoptosis,[33,34] is downregulated for METH-treated mice based on both transcript and protein levels. Consistent with the lack of overlap, there was no significant correlation between relative protein and transcript changes for either MPTP (R ➲ 0.034, p ➲ 0.333) or METH (R ➲ 0.043, p ➲ 0.216). One of the explanations for this low correlation is that neither technique offers high reproducibility to measure relatively small changes (<30%), while the majority of the observed genes do not exhibit large changes at either of the protein or peptide levels. Additionally, translational and post-translational controls may also play a role.

To evaluate the relation between absolute transcript and protein levels, we pooled all three experimental groups (Figure 4E). We estimated absolute protein abundance based on the total number of observations for a given protein by summing the observation peptide count across all five replicates from MPTP and all five from METH. This count measure is an indirect semiquantitative indicator of protein abundance.[24] Transcript levels were determined by averaging the signal intensities across all nine microarray data sets, that is, MPTP, METH, and controls. Despite the lack of overlap between transcripts and proteins regulated by the two neurotoxins, there was a significant positive correlation between absolute protein and transcript abundance for the 1200 genes in common (R ➲ 0.2889, $p < 10^{-21}$). These results suggest that transcript levels can serve as a partial indicator for protein abundance, despite post-transcriptional regulation.

Taking advantage of the protein and mRNA expression data, we examined whether codon usage influenced translational efficiency. Efficiently expressed genes (46 genes) were identified, whose residuals were greater than 2 SD above the LOWESS fitted curve (Figure 4E and Supplementary Table 4 in the Supporting Information). An approximately equal number of genes (43 genes) were identified as inefficiently expressed, with residuals less than 1.4 SD below the curve. A comparison of codon usage revealed that the efficiently translated genes tended to employ more commonly used codons than the inefficiently translated proteins (Supplementary Figure 2 in the Supporting Information).

MicroRNAs (miRNAs) are also thought to play a role in influencing translational efficiency. In both the MPTP- and METH-treated animals, we identified miRNAs (7 and 23 miRNAs, respectively), whose targeted genes showed significantly different expression levels between treated and untreated striata (Supplementary Table 5 in the Supporting Information). A large number of target genes for each miRNA (hundreds) were modestly repressed (1–2%) in the treated samples compared to the control. This subtle repression of many target genes is thought to be characteristic of miRNA regulation.[35] One of the miRNAs (has_mir_570) was significant in both treatment conditions, suggesting a possible shared translational regulatory mechanism.

Functional Implications of the Regulated Genes/Proteins

Despite the low overlap between the transcript and protein data, the combined data provide a total of 195 altered genes following the two neurotoxin treatments, giving a more complete picture of expression regulation in the striatum. These regulated genes/proteins are implicated in a number of functional categories, including mitochondrial dysfunction/ oxidative phosphorylation, oxidative stress, apoptosis/cell death, neurotransmission, and signal transduction (Table 2).

Downregulation for a number of genes involved in mitochondrial dysfunction was found in both MPTP- and METH-treated mice, including five subunits of complex I and several ATP synthase subunits, suggesting mitochondrial dysfunction in the striatum of both MPTP- and METH-treated mice. Cytochrome C1, a known pro-apoptotic protein for neuronal death, was also upregulated in MPTP-treated mice. A previous study demonstrated that complex I deficiency increases the releasable soluble pool of cytochrome C1 in mitochondria.[36] Additionally, both F- and V-type ATPase complexes were significantly downregulated using GSEA (Supplementary Figure 3A in the Supporting Information). Downregulation of F-type ATPase subunits is indeed in concordance with mitochondrial dysfunction and a decrease in ATP production. At the same time, although V-type ATPase is not involved in ATP biosynthesis, it is involved in the charging of synaptic vesicles with neurotransmitters.

Oxidative stress is widely considered a major consequence of mitochondrial dysfunction, thus potentially playing an important role in neurodegeneration. [4] Genes with antioxidant activity (Gpx4 and Gstm5), and possibly regulated in response to oxidative damage (Dusp1 and Fos) were downregulated (Table 2). In addition, upregulation for several other oxidative stress response proteins, PI3K, Usp14, and Rras2, was observed. Rras2 has been previously suggested to regulate oxide species production. [37] PI3K has also been shown to have a role in regulating the toxic levels of reactive oxygen species generated by oxidative stress.[38]

Another group of proteins showing a statistically significant increase in abundance were related to ubiquitin-mediated protein degradation (Supplementary Figure 3B in the Supporting Information). An interesting feature of this group is that it contains both proteins associated with ubiquitin–ligation activity and proteins from the proteasome subunits. While most of the ubiquitin ligases showed upregulation, all four proteasome subunit proteins showed concordant abundance decreases following drug treatment. Overall, the data suggested that generalized cell destruction or degradation of misfolded proteins plays a prominent role in these mouse models of PD.

Discussion

Defining the molecular changes in the striatum of PD brains is necessary to understand the disorder and design of new therapeutic approaches. Microarrays have been used in other papers to analyze the striatum in mouse models of PD.[6-8,39-42] However, differing toxins, doses, and time points in these studies complicate the identification of a reliable profile

specific for PD in mice. We designed an approach using two neurotoxins, MPTP and METH, which each induce Parkinsonism in mice but have distinct mechanisms of action. Changes in common to both neurotoxins may represent a more confident molecular signature of PD, while changes specific to each neurotoxin may reflect their individual toxicology. While it is not entirely known whether the 7 day time point is best for measuring the differences between the two drugs, a significant loss of DA in the target organ, the striatum, is observed in both the MPTP and METH models of PD.

To gain deeper insights into the cellular response of the two neurotoxins, we assayed transcript and protein levels for both agents using microarrays and global quantitative proteomics. These techniques identified a number of significantly up- and downregulated transcripts and proteins in response to MPTP and METH. Some of the significantly regulated proteins may represent a protein group containing several isoforms with the common peptide detected. The current approach cannot pinpoint exactly which isoform(s) contributed to the observed changes, and orthogonal approaches will be necessary to validate the differences. The regulated genes/proteins may be attractive candidates for biomarker development in PD.

High correlations were found between proteins only or between transcripts only in response to MPTP and METH, suggesting that the general cellular response to both neurotoxins is similar. Somewhat surprisingly though, a low correlation was observed between the proteomics and microarray data in each of the neurotoxin models. Only two genes (Gpx4 and Gfap) overlapped between the regulated gene lists of proteomics and microarrays. The low concordance between microarray and proteomic data could be due to multiple factors, including translational and post-translational regulations. It is also possible that the differences in the quantification accuracy and the ability to detect low abundance genes for the two technologies play a major role in the observed low concordance. Most genes detected by global proteomics are relatively abundant because of the dynamic range limitation of current proteomic technologies;[43] however, our results demonstrate the ability to detect as low as ~30% abundance changes exemplified by the Pcp4 protein. Low percentage changes in protein abundances could mean even smaller mRNA changes, which may not be detectable.

Another possibility for the low correlation may be the different mechanisms of the two neurotoxins. For example, we observed nearly a 6-fold decrease in protein abundances for aldehyde dehydrogenase gene Aldh1a1, a gene specifically expressed in dopamine neurons,[44] in MPTP-treated mice but only a 3-fold decrease in METH-treated mice. MPTP causes cell death in neurons that project to the striatum, while METH suspends cell function and DA production without killing the cells. This difference may account for the more severe decrease in protein observed in the MPTP-treated mice.

Our investigation also evaluated proteins to better understand the relationship between transcript and protein levels in the striatum following the loss of dopaminergic afferents. A total of 1614 proteins were confidently identified, and very good consistency was found between replicates and neurotoxins. Differentially regulated proteins in response to drug treatment were also similar.

Interestingly, the Gfap protein was found to be upregulated in response to both MPTP and METH treatment, congruent with the microarray results. There were a number of other proteins that showed a similar response to both toxins. One protein with increased levels was spermidine synthase (Srm), which enhances A*f3*-induced neurotoxicity through increased free-radical levels.[45] As mentioned before, the Aldh1a1 protein was downregulated in response to both neurotoxins and is of particular interest because decreasing Aldh1a1 in

human lens epithelial cells using siRNA increases the susceptibility of the cells to oxidative damage and apoptosis.[46]

To explore the relationship between transcript and protein abundance, we examined the absolute intensity for transcript expression across all experiments and compared them to the protein abundance levels for the 1200 genes in common between the MPTP and METH experiments. Although there were individual cases in which as much as a 26-fold abundance difference could be found between protein and transcript levels, a significant correlation ($p < 10^{-21}$) between proteins and transcripts was found, suggesting that transcript levels can be used as a general indicator of protein abundance.

Our results also identified a number of proteins functionally associated with apoptosis and cell death. In general, downregulation of antiapoptotic proteins and upregulation of pro-apoptotic proteins were observed, although apoptosis is a process in which cellular localization may play as much of a role as the expression level of these factors.[47] Increased apoptosis and cell death factors are likely the consequence of mitochondrial dysfunction and oxidative damage. Indeed, many of the proteins involved in mitochondrial dysfunction and oxidative damage are also suggested to play a role in apoptosis. For example, proteins Gpx4 and Gstm5, which function primarily as antioxidants also have a protective effect against apoptosis.[33,34] Both proteins were downregulated. In addition, antiapoptotic mitochondrial heat-shock protein 10 kDa (Hspe1) had significant reduced protein abundances in both mouse models, again suggesting reduced protection against cell death. Conversely, the pro-apoptotic protein cytochrome C1 (Cyc1) was upregulated in MPTP-treated mice, also as a result of mitochondrial dysfunction. Consistent with these observations, oxidative stress and mitochondrial dysfunction are implicated as major contributors to Parkinsonism in both MPTP-[48] and METH-treated[49,50] mice.

A number of proteins (Table 2) previously implicated in pro-apoptotic activity were observed with increased protein or transcript abundances in both mouse models. For instance, the classic glycolytic protein glyceraldehyde-3-phosphate dehydrogenase (Gapdh) has been identified as a general mediator of one or more apoptotic cascades and promotes Lewy body formation.[51] Cyc1 and Gapdh were only observed with significant abundance increases in MPTP-treated mice, suggesting a potentially higher level of oxidative damage and cell death. The upregulation of the calpain-2 (Capn2) protein in both MPTP- and METH-treated mice is indicative of increased endoplasmic reticulum (ER) stress. Capn2 protein is known to be pro-apoptotic through activation of caspase-12.[52] Increased Capn2 expression and neuronal death in MPTP-treated mice has been previously observed.[53]

Importantly, microarray and proteomic measurements seem to be complementary by providing two different sets of regulated genes. The combined regulated gene and protein list provides a much clearer picture of the biological changes occurring in the striatum following the two drug treatments. Overall, our data provide clear evidence on mitochondrial dysfunction, increased oxidative stress and damage, misregulated protein degradation, increased apoptosis and cell death, and the potential activation of the astrocytic response. While we have focused on aspects of neurotoxicity, other protein or gene expression changes may be related to the loss of dopamine signaling in the striatum. Many of the novel proteins and genes may represent interesting targets for therapeutic intervention or further mechanistic studies. The discovery of common changes helped illuminate pathways relevant to PD, but pathways specific for each toxin were also uncovered. The use of transcript and protein profiling to identify the molecular changes occurring in toxins with similar pathophysiological end effects may be a general approach for differentiating the molecular pathology of disease models from agent-specific effects.

Our data shows that understanding mRNA changes is not enough, and further investigation using multimodal analysis will provide a clearer picture of what is happening in the mouse brain. Because the current AMT method may fail to identify post-translational modifications, subsequent proteomic analyses will use newer technology to include potential modifications into its AMT tag database.[54] In addition, a time-course study will illuminate the evolving changes to the neurotoxins in the mouse brain, while a chronic drug-delivery system might better replicate damage caused by drug abuse in humans.

Supplementary Material

Refer to Web version on PubMed Central for supplementary material.

Acknowledgments

This work was supported by the NIH (RO1 DA015802 and U24 NS052108 to D.J.S. and RO1 NS050148 to D.J.S. and R.D.S.), Staglin Music Festival and NARSAD Young Investigator Award, Tobacco-Related Disease Research Program (11RT-0172), and Alzheimer's Association (IIRG-02-3609 to D.J.S.). PNNL efforts were supported by the NIH National Center for Research Resources (RR18522 to R.D.S.), and proteomics measurements were performed in the Environmental Molecular Sciences Laboratory, a U.S. Department of Energy national scientific user facility located at PNNL in Richland, Washington. PNNL is a multiprogram national laboratory operated by Battelle Memorial Institute for the DOE under Contract DE-AC05-76RL01830.

References

1. Bernheimer H, Birkmayer W, Hornykiewicz O, Jellinger K, Seitelberger F. Brain dopamine and the syndromes of Parkinson and Huntington. Clinical, morphological and neurochemical correlations. J Neurol Sci. 1973; 20(4):415–455. [PubMed: 4272516]
2. Marsden CD. Parkinson's disease. Lancet. 1990; 335(8695):948–952. [PubMed: 1691427]
3. Gandhi S, Wood NW. Molecular pathogenesis of Parkinson's disease. Hum Mol Genet. 2005; 14(18):2749–2755.
4. Lin MT, Beal MF. Mitochondrial dysfunction and oxidative stress in neurodegenerative diseases. Nature. 2006; 443(7113):787–795. [PubMed: 17051205]
5. Ginsberg SD, Hemby SE, Lee VM, Eberwine JH, Trojanowski JQ. Expression profile of transcripts in Alzheimer's disease tangle-bearing CA1 neurons. Ann Neurol. 2000; 48(1):77–87. [PubMed: 10894219]
6. Miller RM, Federoff HJ. Microarrays in Parkinson's disease: A systematic approach. NeuroRx. 2006; 3(3):319–326. [PubMed: 16815215]
7. Miller RM, Chen LL, Kiser GL, Giesler TL, Kaysser-Kranich TM, Palaniappan C, Federoff HJ. Temporal evolution of mouse striatal gene expression following MPTP injury. Neurobiol Aging. 2005; 26(5):765–775. [PubMed: 15708451]
8. Grunblatt E, Mandel S, Maor G, Youdim MB. Gene expression analysis in *N*-methyl-4-phenyl-1,2,3,6-tetrahydropyridine mice model of Parkinson's disease using cDNA microarray: Effect of *R*-apomorphine. J Neurochem. 2001; 78(1):1–12. [PubMed: 11432968]
9. Mandel S, Grunblatt E, Maor G, Youdim MB. Early and late gene changes in MPTP mice model of Parkinson's disease employing cDNA microarray. Neurochem Res. 2002; 27(10):1231–1243. [PubMed: 12462421]
10. Wang H, Qian WJ, Chin MH, Petyuk VA, Barry RC, Liu T, Gritsenko MA, Mottaz HM, Moore RJ, Camp Ii DG, Khan AH, Smith DJ, Smith RD. Characterization of the mouse brain proteome using global proteomic analysis complemented with cysteinyl-peptide enrichment. J Proteome Res. 2006; 5(2):361–369. [PubMed: 16457602]
11. Palacino JJ, Sagi D, Goldberg MS, Krauss S, Motz C, Wacker M, Klose J, Shen J. Mitochondrial dysfunction and oxidative damage in parkin-deficient mice. J Biol Chem. 2004; 279(18):18614–18622. [PubMed: 14985362]
12. Dauer W, Przedborski S. Parkinson's disease: Mechanisms and models. Neuron. 2003; 39(6):889–909. [PubMed: 12971891]

13. Przedborski S, Vila M. The 1-methyl-4-phenyl-1,2,3,6-tetrahydropyridine mouse model: A tool to explore the pathogenesis of Parkinson's disease. Ann N Y Acad Sci. 2003; 991:189–198. [PubMed: 12846987]
14. Lotharius J, Brundin P. Pathogenesis of Parkinson's disease: Dopamine, vesicles and R-synuclein. Nat Rev Neurosci. 2002; 3(12):932–942. [PubMed: 12461550]
15. Cadet JL. Molecular neurotoxicological models of Parkinsonism: Focus on genetic manipulation of mice. Parkinsonism Relat Disord. 2001; 8(2):85–90. [PubMed: 11489672]
16. Kita T, Wagner GC, Nakashima T. Current research on methamphetamine-induced neurotoxicity: Animal models of monoamine disruption. J Pharmacol Sci. 2003; 92(3):178–195. [PubMed: 12890883]
17. Sulzer D, Sonders MS, Poulsen NW, Galli A. Mechanisms of neurotransmitter release by amphetamines: A review. Prog Neurobiol. 2005; 75(6):406–433. [PubMed: 15955613]
18. Melega WP, Raleigh MJ, Stout DB, Lacan G, Huang SC, Phelps ME. Recovery of striatal dopamine function after acute amphetamine- and methamphetamine-induced neurotoxicity in the vervet monkey. Brain Res. 1997; 766(1–2):113–120. [PubMed: 9359594]
19. Sonsalla PK, Jochnowitz ND, Zeevalk GD, Oostveen JA, Hall ED. Treatment of mice with methamphetamine produces cell loss in the substantia nigra. Brain Res. 1996; 738(1):172–175. [PubMed: 8949944]
20. Vijitruth R, Liu M, Choi DY, Nguyen XV, Hunter RL, Bing G. Cyclooxygenase-2 mediates microglial activation and secondary dopaminergic cell death in the mouse MPTP model of Parkinson's disease. J Neuroinflammation. 2006; 3:6. [PubMed: 16566823]
21. Qian WJ, Monroe ME, Liu T, Jacobs JM, Anderson GA, Shen Y, Moore RJ, Anderson DJ, Zhang R, Calvano SE, Lowry SF, Xiao W, Moldawer LL, Davis RW, Tompkins RG, Camp DG II, Smith RD. Quantitative proteome analysis of human plasma following in vivo lipopolysaccharide administration using $^{16}O/^{18}O$ labeling and the accurate mass and time tag approach. Mol Cell Proteomics. 2005; 4(5):700–709. [PubMed: 15753121]
22. Liu T, Qian WJ, Strittmatter EF, Camp DG, Anderson GA, Thrall BD, Smith RD. High-throughput comparative proteome analysis using a quantitative cysteinyl-peptide enrichment technology. Anal Chem. 2004; 76(18):5345–5353. [PubMed: 15362891]
23. Nesvizhskii AI, Keller A, Kolker E, Aebersold R. A statistical model for identifying proteins by tandem mass spectrometry. Anal Chem. 2003; 75(17):4646–4658. [PubMed: 14632076]
24. Qian WJ, Jacobs JM, Camp DG, Monroe ME, Moore RJ, Gritsenko MA, Calvano SE, Lowry SF, Xiao W, Moldawer LL, Davis RW, Tompkins RG, Smith RD. Comparative proteome analyses of human plasma following in vivo lipopolysaccharide administration using multidimensional separations coupled with tandem mass spectrometry. Proteomics. 2005; 5(2):572–584. [PubMed: 15627965]
25. Benjamini Y, Hochberg Y. Controlling the false discovery rate: A practical and powerful approach to multiple testing. J R Stat Soc Ser B. 1995; 57(1):289–300.
26. Storey JD, Tibshirani R. Statistical significance for genomewide studies. Proc Natl Acad Sci U S A. 2003; 100(16):9440–9445. [PubMed: 12883005]
27. Mootha VK, Lindgren CM, Eriksson KF, Subramanian A, Sihag S, Lehar J, Puigserver P, Carlsson E, Ridderstrale M, Laurila E, Houstis N, Daly MJ, Patterson N, Mesirov JP, Golub TR, Tamayo P, Spiegelman B, Lander ES, Hirschhorn JN, Altshuler D, Groop LC. PGC-1R-responsive genes involved in oxidative phosphorylation are coordinately downregulated in human diabetes. Nat Genet. 2003; 34(3):267–273. [PubMed: 12808457]
28. Al-Shahrour F, Minguez P, Tarraga J, Montaner D, Alloza E, Vaquerizas JM, Conde L, Blaschke C, Vera J, Dopazo J. BABELOMICS: A systems biology perspective in the functional annotation of genome-scale experiments. Nucleic Acids Res. 2006; 34:W472–W476. [PubMed: 16845052]
29. Jiang Z, Gentleman R. Extensions to gene set enrichment. Bioinformatics. 2007; 23(3):306–313. [PubMed: 17127676]
30. Skold K, Svensson M, Nilsson A, Zhang X, Nydahl K, Caprioli RM, Svenningsson P, Andren PE. Decreased striatal levels of PEP-19 following MPTP lesion in the mouse. J Proteome Res. 2006; 5(2):262–269. [PubMed: 16457591]

31. Himeda T, Watanabe Y, Tounai H, Hayakawa N, Kato H, Araki T. Time dependent alterations of co-localization of S100*f3* and GFAP in the MPTP-treated mice. J Neural Transm. 2006; 113(12): 1887–1894. [PubMed: 16736245]
32. Lin RC, Polsky K, Matesic DF. Expression of γ-aminobutyric acid immunoreactivity in reactive astrocytes after ischemiainduced injury in the adult forebrain. Brain Res. 1993; 600(1):1–8. [PubMed: 8422577]
33. Ran Q, Gu M, Van Remmen H, Strong R, Roberts JL, Richardson A. Glutathione peroxidase 4 protects cortical neurons from oxidative injury and amyloid toxicity. J Neurosci Res. 2006; 84(1): 202–208. [PubMed: 16673405]
34. Ran Q, Liang H, Gu M, Qi W, Walter CA, Roberts LJ, Herman B, Richardson A, Van Remmen H. Transgenic mice overexpressing glutathione peroxidase 4 are protected against oxidative stress-induced apoptosis. J Biol Chem. 2004; 279(53):55137–55146. [PubMed: 15496407]
35. Pillai RS. MicroRNA function: Multiple mechanisms for a tiny RNA. RNA. 2005; 11(12):1753–1761. [PubMed: 16314451]
36. Perier C, Tieu K, Guegan C, Caspersen C, Jackson-Lewis V, Carelli V, Martinuzzi A, Hirano M, Przedborski S, Vila M. Complex I deficiency primes Bax-dependent neuronal apoptosis through mitochondrial oxidative damage. Proc Natl Acad Sci U S A. 2005; 102(52):19126–19131. [PubMed: 16365298]
37. Lee AC, Fenster BE, Ito H, Takeda K, Bae NS, Hirai T, Yu ZX, Ferrans VJ, Howard BH, Finkel T. Ras proteins induce senescence by altering the intracellular levels of reactive oxygen species. J Biol Chem. 1999; 274(12):7936–7940. [PubMed: 10075689]
38. Goldshmit Y, Erlich S, Pinkas-Kramarski R. Neuregulin rescues PC12-ErbB4 cells from cell death induced by H_2O_2. Regulation of reactive oxygen species levels by phosphatidylinositol 3-kinase. J Biol Chem. 2001; 276(49):46379–46385. [PubMed: 11590144]
39. Cuadrado-Tejedor M, Sesma MT, Gimenez-Amaya JM, Ortiz L. Changes in cytoskeletal gene expression linked to MPTP-treatment in mice. Neurobiol Dis. 2005; 20(3):666–672. [PubMed: 16005240]
40. Fuller RW, Hemrick-Luecke SK. Mechanisms of MPTP (1-methyl-4-phenyl-1,2,3,6-tetrahydropyridine) neurotoxicity to striatal dopamine neurons in mice. Prog Neuropsychopharmacol Biol Psychiatry. 1985; 9(5–6):687–690. [PubMed: 3878976]
41. Mandel S, Grunblatt E, Youdim M. cDNA microarray to study gene expression of dopaminergic neurodegeneration and neuroprotection in MPTP and 6-hydroxydopamine models: Implications for idiopathic Parkinson's disease. J Neural Transm. 2000; (Suppl 60):117–124.
42. Perese DA, Ulman J, Viola J, Ewing SE, Bankiewicz KS. A 6-hydroxydopamine-induced selective parkinsonian rat model. Brain Res. 1989; 494(2):285–293. [PubMed: 2528389]
43. Qian WJ, Jacobs JM, Liu T, Camp DG, Smith RD. Advances and challenges in liquid chromatography–mass spectrometry-based proteomics profiling for clinical applications. Mol Cell Proteomics. 2006; 5(10):1727–1744. [PubMed: 16887931]
44. Galter D, Buervenich S, Carmine A, Anvret M, Olson L. ALDH1 mRNA: Presence in human dopamine neurons and decreases in substantia nigra in Parkinson's disease and in the ventral tegmental area in schizophrenia. Neurobiol Dis. 2003; 14(3):637–647. [PubMed: 14678778]
45. Yatin SM, Yatin M, Varadarajan S, Ain KB, Butterfield DA. Role of spermine in amyloid *f3*-peptide-associated free radical-induced neurotoxicity. J Neurosci Res. 2001; 63(5):395–401. [PubMed: 11223914]
46. Choudhary S, Xiao T, Vergara LA, Srivastava S, Nees D, Piatigorsky J, Ansari NH. Role of aldehyde dehydrogenase isozymes in the defense of rat lens and human lens epithelial cells against oxidative stress. Invest Ophthalmol Vis Sci. 2005; 46(1):259–267. [PubMed: 15623782]
47. Shaul YD, Seger R. The MEK/ERK cascade: From signaling specificity to diverse functions. Biochim Biophys Acta. 2007; 1773(8):1213–1226. [PubMed: 17112607]
48. Fukae J, Mizuno Y, Hattori N. Mitochondrial dysfunction in Parkinson's disease. Mitochondrion. 2007; 7(1–2):58–62. [PubMed: 17300997]
49. Boger HA, Middaugh LD, Patrick KS, Ramamoorthy S, Denehy ED, Zhu H, Pacchioni AM, Granholm AC, McGinty JF. Long-term consequences of methamphetamine exposure in young

adults are exacerbated in glial cell line-derived neurotrophic factor heterozygous mice. J Neurosci. 2007; 27(33):8816–8825. [PubMed: 17699663]

50. Yamamoto BK, Zhu W. The effects of methamphetamine on the production of free radicals and oxidative stress. J Pharmacol Exp Ther. 1998; 287(1):107–114. [PubMed: 9765328]
51. Tsuchiya K, Tajima H, Kuwae T, Takeshima T, Nakano T, Tanaka M, Sunaga K, Fukuhara Y, Nakashima K, Ohama E, Mochizuki H, Mizuno Y, Katsube N, Ishitani R. Pro-apoptotic protein glyceraldehyde-3-phosphate dehydrogenase promotes the formation of Lewy body-like inclusions. Eur J Neurosci. 2005; 21(2):317–326. [PubMed: 15673432]
52. Jayanthi S, Deng X, Noailles PA, Ladenheim B, Cadet JL. Methamphetamine induces neuronal apoptosis via cross-talks between endoplasmic reticulum and mitochondria-dependent death cascades. FASEB J. 2004; 18(2):238–251. [PubMed: 14769818]
53. Chera B, Schaecher KE, Rocchini A, Imam SZ, Sribnick EA, Ray SK, Ali SF, Banik NL. Immunofluorescent labeling of increased calpain expression and neuronal death in the spinal cord of 1-methyl-4-phenyl-1,2,3,6-tetrahydropyridine -treated mice. Brain Res. 2004; 1006(2):150–156. [PubMed: 15051518]
54. Sacksteder CA, Qian WJ, Knyushko TV, Wang H, Chin MH, Lacan G, Melega WP, Camp DG, Smith RD, Smith DJ, Squier TC, Bigelow DJ. Endogenously nitrated proteins in mouse brain: Links to neurodegenerative disease. Biochemistry. 2006; 45(26):8009–8022. [PubMed: 16800626]

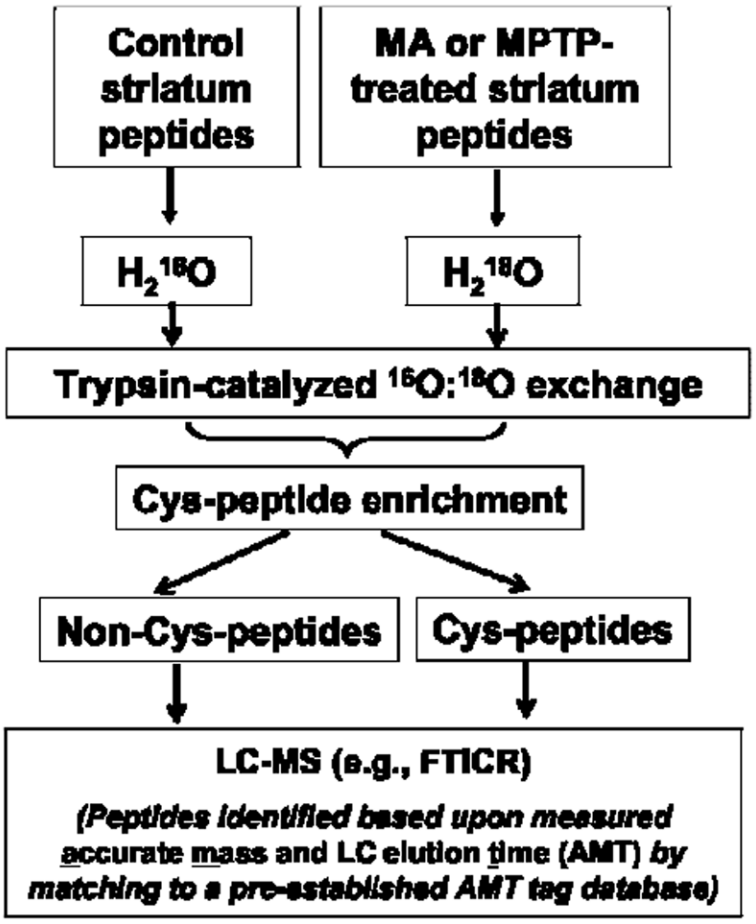

Figure 1. Flowchart showing the experimental strategy

Mouse striata are prepared using a combination of global tryptic digestion, $^{16}O/^{18}O$ labeling, and CPE methodology, followed by LC–FTICR analysis of each fraction and peptide/protein identification using the AMT tag approach.

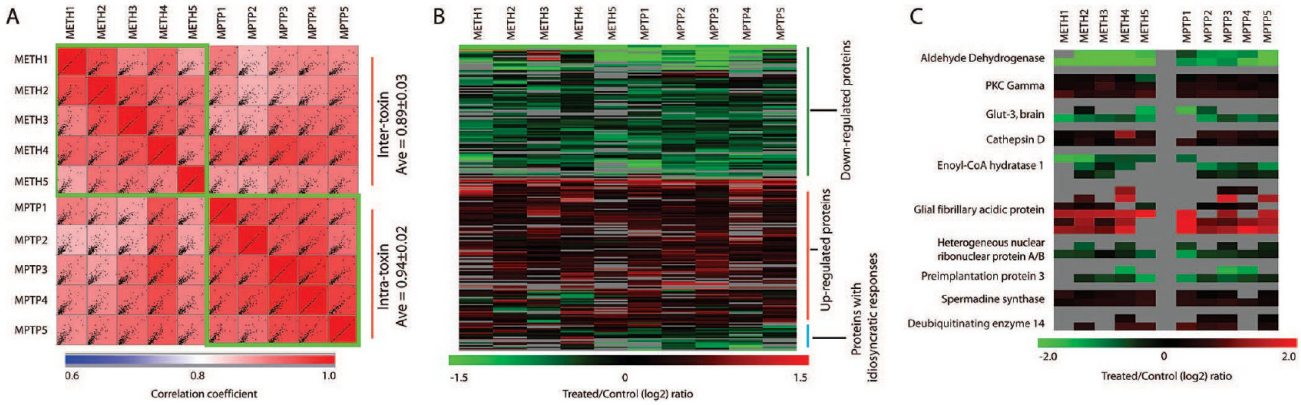

Figure 2. Reproducibility of proteomic analysis

(A) Correlation plots comparing protein expression ratios for the five MPTP and METH replicates relative to controls. This comparison demonstrates significantly similar inter- and intratoxin response at the protein level (R ☽ 0.91 and 0.89, respectively). (B) Heatmap of proteins identified as significantly differentially regulated ($p < 0.05$). The regulated proteins show consistency across samples. (C) Multiple peptides detected from individual proteins show good consistency in expression levels.

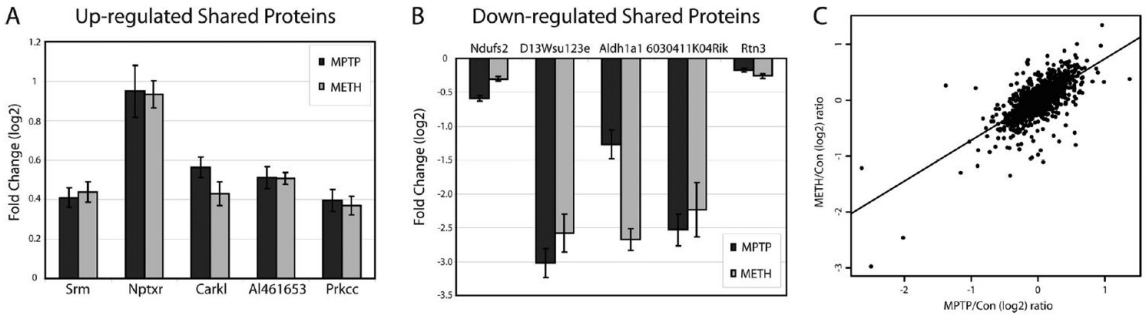

Figure 3. Proteins regulated by MPTP and METH

(A) Proteins that have significant upregulation ($p < 0.05$) in response to both MPTP and METH treatment in the striatum. These are the five top-ranked proteins selected from the combined MPTP and METH data. The graph shows separate data for the two neurotoxins. (B) Top five significantly downregulated proteins in response to both drug treatments. (C) Protein abundances in MPTP- and METH-treated striata compared to controls for all detected peptides passing initial quality control. The Spearman correlation coefficient (R ☽ 0.6563) is significant ($p < 10^{-20}$).

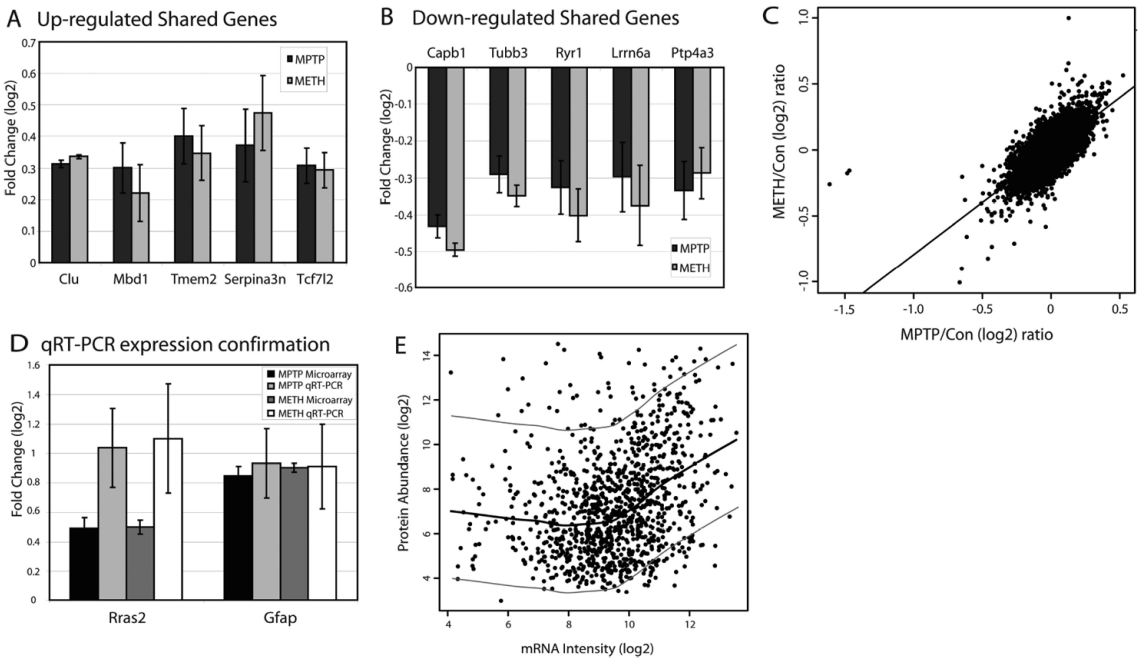

Figure 4. Microarray analysis reveals genes regulated in common in MPTP- and METH-treated striata

(A) Upregulated genes shared by both treatment groups (MPTP and METH). These are the five top-ranked genes selected from the combined MPTP and METH data. The graph shows separate data for the two neurotoxins. (B) Top five genes found to be significantly downregulated in response to both drug treatments. (C) Gene expression ratios (treatment over control) are compared across MPTP and METH treatments ($R \sim 0.718$, $p < 10^{-16}$). (D) Selected gene expression levels confirmed using quantitative real-time polymerase chain reaction (qRT-PCR) ($p < 0.05$, all tests). (E) mRNA levels compared to protein abundance. A scatter plot comparing protein to mRNA levels averaged across treated and control samples. LOWESS fitted curve (dark line) ($R \sim 0.289$, $p < 10^{-21}$). Efficiently transcribed genes lie > 2 standard deviations (SD) above the LOWESS curve (upper gray line indicates 2 SD cutoff), and inefficiently transcribed genes lie < 1.4 SD below the curve (lower gray line).

Table 1

Significant Protein Changes

IPI reference	gene symbol	protein name	MPTP ratio	METH ratio
IPI00123276.1	2810484M10Rik	MOCO sulfurase C-terminal domain containing 2	0.32	0.51
IPI00311818.1	Adh5	alcohol dehydrogenase 5	0.38	0.25
IPI00380501.2	Aldh1a1	aldehyde dehydrogenase family 1, A1	−1.27	−2.68
IPI00153317.2	Aldh1l1	10-formyltetrahydrofolate dehydrogenase	0.62	0.51
IPI00271986.3	Atp5j2	ATP synthase f chain, mitochondrial	−0.67	−0.41
IPI00118787.1	Atp6v1d	ATPase, H^+ transporting, lysosomal V1 subunit D	−0.55	−0.34
IPI00127598.1	Atpif1	ATPase inhibitory factor 1	−0.47	−0.45
IPI00226771.2	Bri3bp	BRI3 binding protein	−0.63	0.11
IPI00119618.1	Canx	calnexin precursor	−0.57	−0.30
IPI00308938.3	Capn2	calpain-2 catalytic subunit precursor	0.39	0.38
IPI00111265.1	Capza2	F-actin capping protein subunit R-2	0.35	0.02
IPI00116277.1	Cct4	T-complex protein 1 subunit delta	0.35	0.30
IPI00330192.1	Cnk2	MKIAA0902 protein	0.36	0.23
IPI00338452.2	Col4a2	collagen R-2(IV) chain precursor	−0.40	−0.32
IPI00131871.1	Cops4	COP9 complex S4	0.22	0.41
IPI00111013.1	Ctsd	cathepsin D precursor	0.47	0.44
IPI00129146.1	Cugbp2	CUG triplet repeat, RNA binding protein 2	−0.27	−0.12
IPI00132728.1	Cyc1	cytochrome C1 heme protein, mitochondrial precursor	0.34	0.03
IPI00119945.1	D16Ertd502e	nitrilase family, member 2	0.44	0.33
IPI00116112.1	Dctn2	dynactin subunit 2	−0.32	0.24
IPI00331549.1	Dhrs1	dehydrogenase/reductase SDR family member 1	0.22	0.43
IPI00221795.1	Echs1	enoyl coenzyme A hydratase	−0.51	−0.84
IPI00135677.1	Ehd3	EH domain-containing protein 3	0.45	0.40
IPI00318496.1	Gad1	glutamate decarboxylase 1	0.48	0.30
IPI00318522.3	Gad2	glutamate decarboxylase 2	0.23	−0.45
IPI00279548.2	Gapdh	similar to glyceraldehyde-3-phosphate dehydrogenase	0.23	0.12
IPI00404368.1	GFAP	glial fibrillary acidic protein	1.16	0.94
IPI00338854.1	Gnai3	guanine nucleotide-binding protein G(k) R	−0.29	−0.46
IPI00115544.1	Gng4	guanine nucleotide-binding protein G	0.47	−0.23
IPI00119952.1	Gpm6b	neuronal membrane glycoprotein M6-b	−0.32	−0.45
IPI00117281.1	GPX4	phospholipid hydroperoxide glutathione peroxidase	−0.16	−0.25
IPI00114380.1	Gstm5	glutathione *S*-transferase Mu 5	−0.54	−0.61
IPI00228828.3	Guk1	guanylate kinase	0.27	0.64
IPI00133034.1	Hint2	histidine triad nucleotide binding protein 2	0.43	0.18
IPI00230730.1	Hist2h3c2	histone cluster 2, H3c2	−0.49	−0.51
IPI00117288.1	Hnrpab	heterogeneous nuclear ribonucleoprotein A/B	−0.51	−0.52
IPI00221788.1	Hpcal4	hippocalcin-like 4	0.58	0.53
IPI00123802.2	Hsp110	heat-shock protein 105 kDa	0.26	0.11
IPI00263863.4	Hspe1	10 kDa heat-shock protein, mitochondrial	−0.28	−0.44

IPI reference	gene symbol	protein name	MPTP ratio	METH ratio
IPI00322447.1	Igsf4a	immunoglobulin superfamily, member 4A	0.84	0.39
IPI00321348.2	Igsf8	immunoglobulIn superfamily, member 8	−0.29	−0.42
IPI00114801.1	Inpp1	inositol polyphosphate 1-phosphatase	−0.37	−0.21
IPI00119433.1	Ivd	isovaleryl coenzyme A dehydrogenase	0.34	0.38
IPI00315359.1	Kcnab2	voltage-gated potassium channel *f3*-2	0.41	0.02
IPI00124479.1	Kif2a	kinesin-like protein	0.48	0.33
IPI00116896.1	mt-Atp8	ATP synthase protein 8	−0.25	−0.45
IPI00228583.3	Mtpn	myotrophin (V-1 protein)	−1.12	−0.45
IPI00118930.1	Napa	R-soluble NSF attachment protein	−0.53	−0.45
IPI00116748.1	Ndufa10	NADH dehydrogenase [ubiquinone] 1 R 10	−0.33	−0.26
IPI00132531.1	Ndufb5	NADH dehydrogenase [ubiquinone] 1 *f3* 5	−0.56	−0.15
IPI00128023.1	Ndufs2	NADH dehydrogenase [ubiquinone] iron–sulfur 2	−0.58	−0.30
IPI00120232.1	Ndufs7	NADH dehydrogenase [ubiquinone] iron–sulfur 7	−0.58	−0.28
IPI00135659.1	Omg	oligodendrocyte–myelin glycoprotein precursor	−0.40	−0.33
IPI00229996.3	Pcp4	Purkinje cell protein 4	−0.24	−0.44
IPI00126014.1	Pde10a	phosphodiesterase 10A	−0.38	−0.30
IPI00222767.1	Pdhx	pyruvate dehydrogenase complex, component X	0.42	0.20
IPI00380348.1	Pgm2	phosphoglucomutase-1	−0.46	−0.47
IPI00336313.2	Ppp1r9a	protein phosphatase 1, regulatory (inhibitor) 9A	−0.17	−0.86
IPI00109504.1	Prei3	preimplantation protein 3	−0.74	−0.80
IPI00122069.1	Prkcc	protein kinase C, γ type	0.39	0.37
IPI00131548.1	Prosc	proline synthetase cotranscribed bacterial homologue	−0.34	−0.23
IPI00113287.1	Psmd9	26S proteasome non-ATPase regulatory subunit 9	0.21	−0.22
IPI00337980.1	Rab21	Ras-related protein Rab-21	−0.67	−0.10
IPI00263129.4	Rps17	40S ribosomal protein S17	−0.88	0.44
IPI00331345.3	Rps3a	ribosomal protein S3A	0.36	0.33
IPI00153743.1	Sfrs7	splicing factor, arginine/serine-rich 7	0.27	0.36
IPI00134191.3	Slc2a3	solute carrier family 2, facilitated glucose transporter 3	−0.95	−0.93
IPI00125635.1	Snap25	synaptosomal-associated protein, 25 kDa	−0.10	−0.23
IPI00110254.1	snca	synuclein, R	−0.32	−0.33
IPI00136912.1	Srm	spermidine synthase	0.41	0.44
IPI00120344.1	Supt16 h	suppressor of Ty 16 homologue	0.33	−0.16
IPI00129622.3	Syt2	synaptotagmin-2	−0.47	−0.40
IPI00136618.1	Tollip	toll-interacting protein	0.37	0.63
IPI00230044.1	Tpm3	tropomyosin R-3 chain	−0.03	−0.44
IPI00139788.2	Trf	serotransferrin precursor	0.46	0.16
IPI00113430.1	Trim2	tripartite motif-containing protein 2	0.22	−0.22
IPI00222496.1	Txndc7	protein disulfide isomerase P5	0.16	−0.26
IPI00270877.2	Usp14	ubiquitin carboxyl-terminal hydrolase 14	0.52	0.54
IPI00135655.1	Vapb	vesicle-associated membrane protein-associated B	−1.32	−1.21
IPI00387475.1	Wasf1	WAS protein family, member 1	0.39	0.17
IPI00112584.1	Camk2d	calcium/calmodulin-dependent protein kinase II, Δ 2	0.15	0.01

IPI reference	gene symbol	protein name	MPTP ratio	METH ratio
IPI00124778.1	Baiap2	insulin receptor tyrosine kinase substrate–protein p53	−0.51	−0.15
IPI00339766.2	Akap5	similar to A-kinaSe anchor protein 5	−0.32	−0.12
IPI00113690.2	Dst	835 kDa protein	0.28	0.38
IPI00355655.2		similar to opioid binding protein/cell adhesion molecule	0.53	0.46
IPI00348414.1	Gm237	similar to hypothetical protein FLJ14547	0.39	0.48

J Proteome Res. Author manuscript; available in PMC 2012 April 4.

Table 2

Selected Genes/Proteins Implicated in Different Functional Categories[a]

gene	protein name	METH proteomics	MPTP proteomics	METH microarray	MPTP microarray	PUBMED
	Mitochondrial Dysfunction and Oxidative Phosphorylation					
Ndufa10	NADH–ubiquinone oxidoreductase 42 kDa subunit	down (−0.26)[b]	down (−0.33)[b]	down (−0.04)	down (−0.04)	
Ndufb5	NADH–ubiquinone oxidoreductase sgdh subunit	down (−0.15)[b]	down (−0.56)[b]	down (−0.01)	down (−0.07)	
Ndufs2	NADH–ubiquinone oxidoreductase 49 kDa subunit	down (−0.30)[b]	down (−0.58)[b]	down (−0.17)	down (−0.06)	
Ndufs7	NADH–ubiquinone oxidoreductase 20 kDa subunit	down (−0.27)[b]	down (−0.58)[b]	down (−0.04)	down (−0.01)	
Ndufb9	NADH dehydrogenase [ubiquinone] 1 *f*3 subcomplex subunit 9			down (−0.19)[b]	down (−0.14)[b]	
Atp6v1d	vacuolar ATP synthase subunit D	down (−0.34)[b]	down (−0.55)[b]	down (−0.16)	down (−0.16)	
Atp5j2	ATP synthase F chain, mitochondrial	down (−0.40)[b]	down (−0.67)[b]	down (−0.18)	down (−0.15)	
mt-Atp8	ATP synthase protein 8	down (−0.45)[b]	down (−0.25)[b]	down (−0.03)	up (0.05)	
Cyc1	Cytochrome C1, heme protein, mitochondrial	up (0.03)	up (0.33)[b]	down (−0.06)	down (−0.11)	
Atpif1	ATPase inhibitor, mitochondrial	down (−0.45)[b]	down (−0.47)[b]	down (−0.12)	down (−0.11)	
Hspe1	10 kDa heat-shock protein, mitochondrial	down (−0.44)[b]	down (−0.28)[b]	down (−0.07)	down (−0.07)	
	Oxidative Stress Response					
Gpx4	phospholipid hydroperoxide glutathione peroxidase, mitochondrial	down (−0.25)[b]	down (−0.16)	down (−0.21)[b]	down (−0.11)	
Gstm5	glutathione *S*-transferase mu 5	down (−0.60)[b]	down (−0.54)[b]	down (−0.21)	down (−0.12)	
Dusp1	dual specificity protein phosphatase 1			down (−0.31)[b]	down (−0.40)[b]	
Fos	Proto-oncogene protein c-fos			down (−0.33)[b]	down (−0.50)[b]	
Usp14	ubiquitin carboxyl-terminal hydrolase 14	up (0.54)[b]	up (0.52)[b]	up (0.12)	up (0.07)	
Pik3c2a	phosphatidylinositol-4-phosphate 3-kinase c2 domain- containing R polypeptide			up (0.43)[b]	up (0.32)[b]	16155123
Rras2	Ras-related protein r-ras2			up (0.56)[b]	up (0.52)[b]	
Calpain	ER stress	up (0.38)	up (0.39)[b]	up (0.08)	up (0.21)	
	Apoptosis and Cell Death					
Antiapoptosis						
Hspe1	10 kDa heat-shock protein, mitochondrial	down (−0.44)[b]	down (−0.28)[b]	down (−0.07)	down (−0.07)	
Col4a2	collagen R 2(iv) chain	down (−0.33)[b]	down (−0.40)[b]	down (−0.15)	down (−0.09)	

gene	protein name	METH proteomics	MPTP proteomics	METH microarray	MPTP microarray	PUBMED
Napa	R-soluble nsf attachment protein.	down (−0.45)[b]	down (−0.53)[b]	down (−0.16)	down (−0.17)	
Gpx4	phospholipid hydroperoxide glutathione peroxidase	down (−0.25)[b]	down (−0.16)	down (−0.20)[b]	down (−0.11)	
Pcp4	Purkinje cell protein 4, Pep-19	down (−0.43)[b]	down (−0.24)[b]	down (−0.09)	down (−0.12)	16457591
Pro-apoptosis						
CD38	ADP-ribosyl cyclase 1			up (0.30)[b]	up (0.31)[b]	
Clu	clusterin			up (0.33)[b]	up (0.29)[b]	
Ctsd	cathepsin D 12107093	up (0.44)[b]	up (0.48)[b]	up (0.07)	up (0.05)	12811635
Ctss	cathepsin S			up (0.30)[b]	up (0.20)[b]	
Capn2	calpain 2, (m/II) large subunit	up (0.38)[b]	up (0.39)[b]	up (0.08)	up (0.21)	12764095
Rps3a	ribosomal protein S3A	up (0.33)[b]	up (0.36)[b]	down (−0.02)	down (−0.02)	17213182
Sirt2	sirtuin 2	down (−0.02)	up (0.01)	up (0.28)[b]	up (0.27)[b]	
Gapdh	glyceraldehyde-3-phosphate dehydrogenase	up (0.12)	up (0.23)[b]	down (−0.05)	up (0.09)	15673432
Cyc1	cytochrome C1, heme protein, mitochondrial	up (0.03)	up (0.33)[b]	down (−0.06)	down (−0.11)	

[a] All numbers in parenthesis are $\log_2$ format of the ratio (METH/control or MPTP/control). PUBMED IDs indicate the references suggesting that the proteins were associated with PD.

[b] Significant expression change ($p < 0.05$) using Student's t test.